RSC Advances

PAPER

View Article Online
View Journal | View Issue

Cite this: *RSC Adv.*, 2021, **11**, 33613

Hollow ZnO nanorices prepared by a simple hydrothermal method for NO_2 and SO_2 gas sensors

Luu Hoang Minh,[ab] Pham Thi Thuy Thu,[a] Bui Quang Thanh,[a] Nguyen Thi Hanh,[a] Do Thi Thu Hanh,[a] Nguyen Van Toan,[b] Chu Manh Hung,[b] Nguyen Van Duy,[b] Pham Van Tong *[a] and Nguyen Duc Hoa[b]

Received 4th August 2021
Accepted 8th October 2021

DOI: 10.1039/d1ra05912b

rsc.li/rsc-advances

Chemoresistive gas sensors play an important role in detecting toxic gases for air pollution monitoring. However, the demand for suitable nanostructures that could process high sensing performance remains high. In this study, hollow ZnO nanorices were synthesized by a simple hydrothermal method to detect NO_2 and SO_2 toxic gases efficiently. Material characterization by some advanced techniques, such as scanning electron microscopy, transmission electron microscopy, X-ray diffraction, and Raman spectroscopy, demonstrated that the hollow ZnO nanorices had a length and diameter size of less than 500 and 160 nm, respectively. In addition, they had a thin shell thickness of less than 30 nm, formed by an assembly of tiny nanoparticles. The sensor based on the hollow ZnO nanorices could detect low concentration of NO_2 and SO_2 gasses at sub-ppm level. At an optimum operating temperature of 200 °C, the sensor had response values of approximately 15.3 and 4.8 for 1 ppm NO_2 and 1 ppm SO_2, respectively. The sensor also exhibited good stability and selectivity, suggesting that the sensor can be applied to NO_2 and SO_2 toxic gas detection in ambient air.

1. Introduction

Air pollution caused by the emission of highly toxic nitrogen dioxide (NO_2) and sulfur dioxide (SO_2) gases from automobiles, fossil fuel combustion, and forest fires is threatening modern societies.[1–4] NO_2 and SO_2 gases are extremely hazardous because they could directly affect the health of humans and animals.[1,5] Exposure to low concentrations of NO_2 or SO_2 gas can increase the incidence of respiratory diseases, decrease lung function, and increase the risk of respiratory infections. The exposure limits of NO_2 and SO_2 for the human respiratory system are 4 and 5 ppm, respectively. Therefore, high-performance and low-cost gas sensors are crucial for the real-time detection and monitoring of these toxic gases at low concentrations of ppb levels.[6,7]

Substantial research has been conducted on the fabrication of gas sensors for application in monitoring NO_2 and SO_2 gases,[8–13] and chemiresistive sensors are believed to be the most effective one because of its simple structure, high sensitivity, low manufacturing cost, and easy integration with silicon technology.[14–16] Different sensing materials could perform different sensing capabilities for gas sensors;[17–19] thus, many scientists have been working hard to synthesize various materials to increase the sensing performance of gas sensors.[18–20] As a typical n-type semiconductor, ZnO with a wide bandgap (~3.37 eV),[21] has been proven to be suitable for gas sensor applications[22,23] because of its low cost and capability to detect several toxic gases, including of NO_2,[24] SO_2,[25] CO,[26] and NH_3.[27] In recent years, ZnO nanostructures with different morphologies, such as nanoparticles,[28] nanowires,[29] nanoplates,[30] nanobelts,[31] and nanorods,[32] have been synthesized for gas sensors. For instance, Vanalakar *et al.*[33] fabricated ZnO nanorods for the detection of NO_2 gases with a concentration ranging from 20 ppm to 100 ppm. Jiao *et al.*[34] synthesized three different ZnO nanostructures, including dense nanorods, dense nanowires, and sparse nanowires, for gas sensors and found that the sparse nanowires are effective for the detection of NO_2. Liu *et al.*[24] prepared vertically aligned ZnO nanorods for NO_2 gas sensors, and the response value was reported to be approximately 200 toward 5 ppm NO_2 at 250 °C. Zhou *et al.*[35] used ZnO nanoflowers for SO_2 sensors, and a response value of 15 was reported for 30 ppm SO_2 at an optimum working temperature of 260 °C. The ZnO, and CdO–ZnO nanorices were prepared for formaldehyde gas sensing applications,[36] where the materials have a big size with a length and diameter of about 3 μn and 130 nm, respectively, without the hollow structure, leading to low adsorption sites for gas adsorption. Clearly, the gas sensing properties of ZnO are determined by its (i) crystal size, (ii) porosity, (iii) assembly, and (iv) characteristics. Thus, ZnO nanostructures with a porous structure, small crystal size, and large specific surface area are desired to enhance its gas

[a]*Department of Physics, Faculty of Mechanical Engineering, National University of Civil Engineering (NUCE), No. 55, Giai Phong Str., Hanoi, Vietnam. E-mail: tongpv@nuce.edu.vn*

[b]*International Training Institute for Materials Science (ITIMS), Hanoi University of Science and Technology (HUST), No. 1, Dai Co Viet, Hanoi, Vietnam*

responsivity.[34] However, to the best of our knowledge, no study has reported on the synthesis and gas sensing characteristics of ZnO hollow nanorices even though nanostructured ZnO with various morphologies have been extensively investigated. In addition, the development of a scalable and facile method for synthesis of ZnO nanostructures to achieve low-cost sensor fabrication and detection of highly toxic NO_2 and SO_2 gases at low concentrations remains as a big challenge.

Here, we prepared hollow ZnO nanorices by the hydrothermal method without the use of surfactants for NO_2 and SO_2 gas sensors. The hollow ZnO nanorices are advantageous for gas sensing applications because of (i) the ultrathin shell of the ZnO nanorices formed by the assembly of tiny nanoparticles with diameters approximately twice the Debye length and (ii) the hollow structure providing the large specific surface area. The fabricated sensor showed an excellent response to low concentrations (250 ppb) of NO_2 and SO_2 with the values of 4.8, and 2, respectively.

2. Experimental

2.1. Synthesis of hollow ZnO nanorices

The materials used in this study, including of zinc chloride ($ZnCl_2$, 99.9%), D-glucose ($C_6H_{12}O_6 \cdot 6H_2O$, 99.5%), ammonium solution (35%), ethanol (C_2H_5OH), and deionized (DI) water, were analytical grade. Hydrothermal method was used to prepare the hollow ZnO nanorices. Progresses for the preparation of hollow ZnO nanorices are illustrated in Scheme 1. In briefly, 1.36 g of $ZnCl_2$ and 1 g of D-glucose were dissolved in 80 ml of deionized water (DI), and the pH of the solution was adjusted to 10 by adding ammonium solution. Then, mixture solution was poured into a 100 ml Teflon-lined stainless-steel autoclave and sealed. The sealed autoclave was placed in an electric oven and maintained at 160 °C for hydrothermal reaction for 16 h. After the reaction, the electric oven was turned off and led to cool down to room temperature naturally, and the precipitated product was washed by DI water, followed by ethanol. Lastly, the product was collected by centrifuging, and air-dried at 75 °C overnight before use for sensor fabrication and material characterization.

2.2. Sensor fabrication and characterization

For gas sensing measurement, the thick film technique was used to fabricate the gas sensor.[37] Specifically, 5 mg of ZnO powders was dispersed in ethanol solution by bath ultrasonic vibration for approximately 5 min. Then, solution was dropped onto Pt interdigital electrodes, and then heat treated at 550 °C for 2 h in air to stabilize the sensor. To measure the sensor's gas-sensitive characteristics, the sensor was placed on the surface of a heating plate to control the working temperature of the sensor. The resistance of the sensor was continuously measured using the Keithley instrument (Model 2602), while the ambient was changed from air to tested gas. Here, the analysis of NO_2 and SO_2 and the gas concentration was controlled by changes in the mixing ratio of the standard gas (100 ppm, NO_2; 100 ppm, SO_2) with dry air using a mixing system.[38] We difined the sensor response $S = R_{gas}/R_{air}$ for oxidizing gases (NO_2, SO_2) and $S = R_{air}/R_{gas}$ for reducing gases (H_2, CO, NH_3, CO_2). R_{air} is the resistance of the sensor in dry air, whereas R_{gas} is the resistance of the sensor in tested gas.

2.3. Material characterization

The crystal structure of the synthesized material was studied by X-ray diffraction (XRD, Bruker D8 Advance), operated at 40 kV

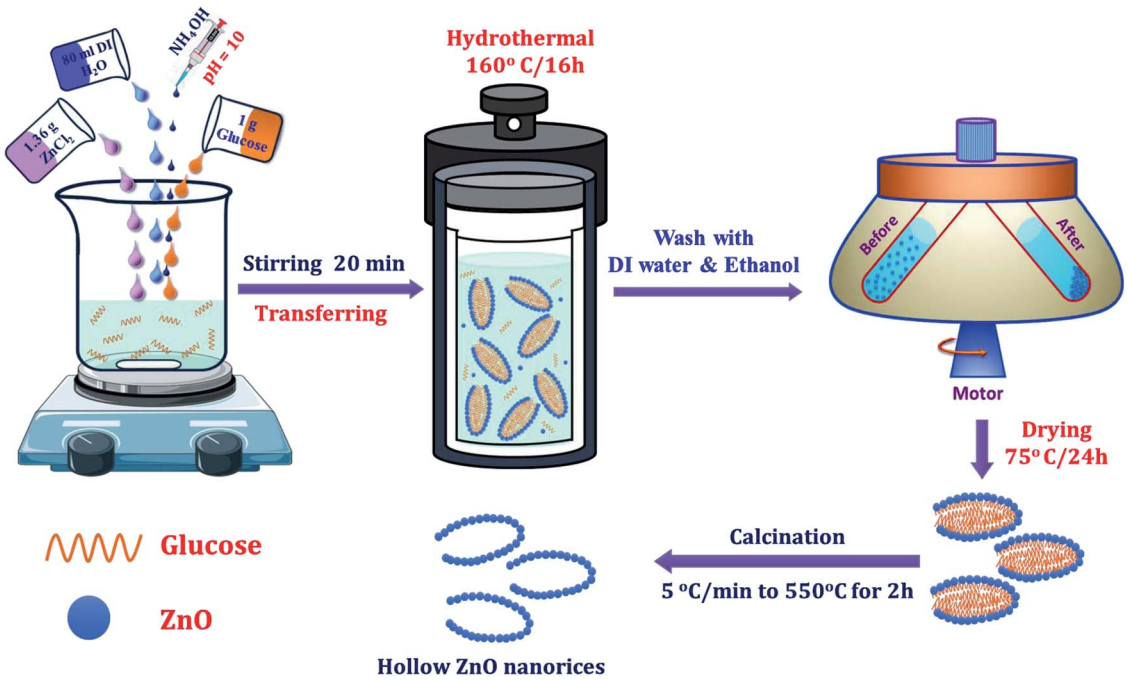

Scheme 1 Processes for the hydrothermal synthesis of hollow ZnO nanorices.

and 40 mA using Cu-Kα radiation (λ = 1.54178 Å) in the 2θ range of 20°–80°. The morphology of the synthesized material was investigated by field emission scanning electron microscopy (FE-SEM; JEOL model 7600F) and transmission electron microscopy (TEM, JEOL 2100F). The atomic composition of the sample was analyzed by energy-dispersive X-ray (EDX) spectroscopy. Raman spectra were measured at room temperature (Renishaw, InVia, excited laser 328 nm). The specific surface area of the synthesized material was calculated on the basis of the isothermal nitrogen adsorption/desorption curve through the BET equation, whereas the pore size of material was determined by the Barrett–Joyner–Halenda (BJH) method applied to the desorption branch of the gravitation isotherm curve.[39]

3. Results and discussion

3.1. Morphology and structure of hollow ZnO nanorices

The surface morphology of the synthesized materials after heat treatment at 550 °C for 2 h in air was observed *via* FE-SEM images, as shown in Fig. 1A–C. The survey FE-SEM image shown in Fig. 1A reveals that the hollow ZnO nanorices have a relatively uniform shape without other morphologies. The average length of the hollow ZnO nanorice is about 500 nm, while its diameter is approximately 160 nm. The surface of the nanorices is not smooth due to the accumulation of tiny nanoparticles. The high-magnification FE-SEM images (Fig. 5B and C) demonstrate that the hollow ZnO nanorices have an open end and a closed end, with a shell thickness of approximately 30 nm. The shell of the nanorice is not smooth but composed of aggregated nanoparticles of less than 30 nm (Fig. 5C). This study is the first to synthesize hollow ZnO nanorices with such thin shell thickness successfully. The formation of hollow ZnO nanorices can be explained as follows: (i) glucose molecules spontaneously agglomerate, acting as a rice-shaped nuclei during the hydrothermal process. (ii) The process of forming ZnO nanocrystals on the surface of agglomerated glucose soft template. The precursors were decomposed to form Zn^{2+} and OH^- and increased during the hydrothermal process at a high temperature of 160 °C. When supersaturation exceeds the limit value, ZnO crystal nuclei begin to form and grow on the rice-shaped agglomerated glucose molecules. (iii) Upon heat treatment at 550 °C/2 h, the glucose templates were completely burned to form the hollow structure of the ZnO nanorices. The decomposition and formation of ZnO crystal nuclei in a hydrothermal environment can be represented by the following reactions:[40]

$$Zn^{2+} + 4OH^- \rightarrow [Zn(OH)_4]^{2-} \quad (1)$$

$$[Zn(OH)_4]^{2-} \leftrightarrow Zn(OH)_2 + 2OH^- \quad (2)$$

$$Zn(OH)_2 \leftrightarrow ZnO + H_2O \quad (3)$$

$$[Zn(OH)_4]^{2-} \leftrightarrow ZnO + 2H_2O + 2OH^- \quad (4)$$

Compositional analysis of the hollow ZnO nanorices was conducted *via* EDX, as shown in Fig. 2D. Data reveal that the sample comprises Zn and O elements. No impurity is observed, indicating the high purity of the ZnO material. The elemental ratio of [O]/[Zn] is 48.6/51.4, which is less than the stoichiometry of ZnO material ([O]/[Zn] = 1.0), confirming the existence of

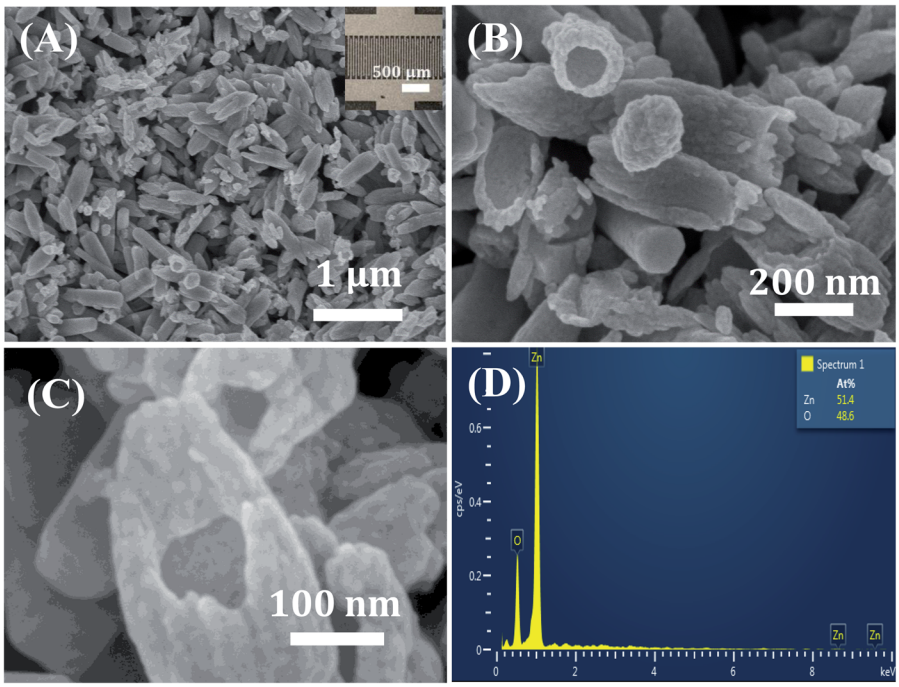

Fig. 1 (A) Low- and (B and C) high-magnification FE-SEM images and (D) EDX spectrum of hollow ZnO nanorices. Inset in (A) is a photo of the fabricated sensor.

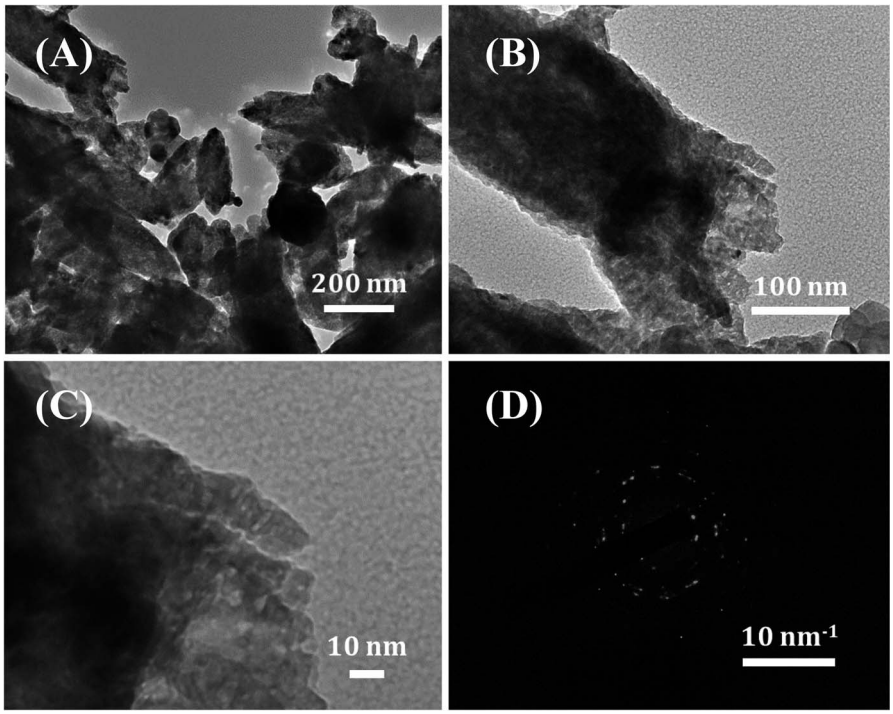

Fig. 2 (A) Low- and (B and C) high-magnification TEM images, and (D) SAED pattern of the hollow ZnO nanorices.

the vacancies of oxygen in the lattice of the hollow ZnO nanorices. Therefore, the hollow ZnO nanorices are expected to show n-type semiconducting behavior for gas sensing applications.

A further investigation on the morphological and crystal characteristics of the hollow ZnO nanorices was conducted using TEM images, as shown in Fig. 2. The low-magnification TEM image (Fig. 2A) shows that the obtained material is shaped like a nanorice with a hollow structure. The shell of the nanorice has the porous nature of an assembly of nanoparticles with many small pores with a size of a few nanometers (Fig. 2B). The high-magnification TEM image (Fig. 2C) on the shell of the hollow ZnO nanorices. The selected area electron diffraction (SAED) pattern (Fig. 2D) reveals the polycrystalline nature of the hollow ZnO nanorices. The results confirm that the shell of the hollow nanorice is assembled from tiny ZnO nanocrystals.

The XRD of the sample obtained after heat treatment at 550 °C/2 h is shown in Fig. 3A. All diffraction peaks are perfectly indexed to the hexagonal (wurtzite) structure of ZnO with lattice parameters $a = b = 3.2498$ Å, $c = 5.2066$ Å, $\alpha = \beta = 90°$, $\gamma = 120°$, space group $P6_3mc$ (JCPDS card no. 36-1451).[41] The diffraction peaks at $2\theta = 31.8°$, 34.5°, 36.4°, 47.5°, 56.7°, 62.4°, 66.7°, 68.0°, 69.2°, 72.6°, and 76.9° correspond to reflections (100), (002), (101), (102), (110), (103), (200), (112), (201), (004), and (202), respectively. The intensity of peak (101) is the highest, indicating the preferred growth direction of ZnO nanocrystals. The average crystallite size of the ZnO nanorices calculated by the Scherrer equation using diffraction peak (101) is approximately 31.52 nm.[42] This result shows that the hollow ZnO nanorices are formed from assembled nanocrystals to form nanorice shells. The hollow structure with the thin thickness of the nanorice shell is advantageous for gas sensor applications because the inner and outer sides of the nanorices can be exposed to the analytic gas in sensor characterization, leading to the sensor response.

Fig. 3B presents the Raman spectrum of the hollow ZnO nanorices measured at room temperature using the excited laser lines (532 nm). All observed spectroscopic peaks at 332, 380, 437, and 586 cm^{-1} can be assigned to the active Raman modes of the ZnO wurtzite structure with a C_{v6} point group symmetry.[43,44] The active Raman mode observed at 437 cm^{-1} has the strongest intensity assigned for the $E_2(H)$ mode, which shows that the synthesized hollow ZnO nanorices have a good quality crystal with perfect hexagonal wurtzite crystal structure.

The nitrogen adsorption/desorption isotherm of the hollow ZnO nanorices is shown in Fig. 4. The nitrogen adsorption/desorption isotherm of the hollow ZnO nanorices exhibits a typical type-IV mesoporous material, which has the characteristic of a hysteresis loop, representing monolayer and multilayer adsorption with capillary condensation.[45] The BET surface area of the hollow ZnO nanorices is approximately 9.44 $m^2 g^{-1}$. This value is approximately 1.4 folds higher than that of the ZnO nanoflowers (6.71 $m^2 g^{-1}$).[46] The pore size distribution estimated from the isothermal desorption branch by the BJH method using the Halsey equation[39] is shown in the inset of Fig. 4. The results show that the pores have a hierarchical structure in the range of 30–60 nm, with the main peak at approximately 27.6 nm. The pore size distribution is consistent with that observed in the FE-SEM images.

3.2. Electrical and gas sensing properties

Fig. 5A shows the current–voltage (*I–V*) plots of the hollow ZnO nanorice sensor. The *I–V* curves measured in dry air show that

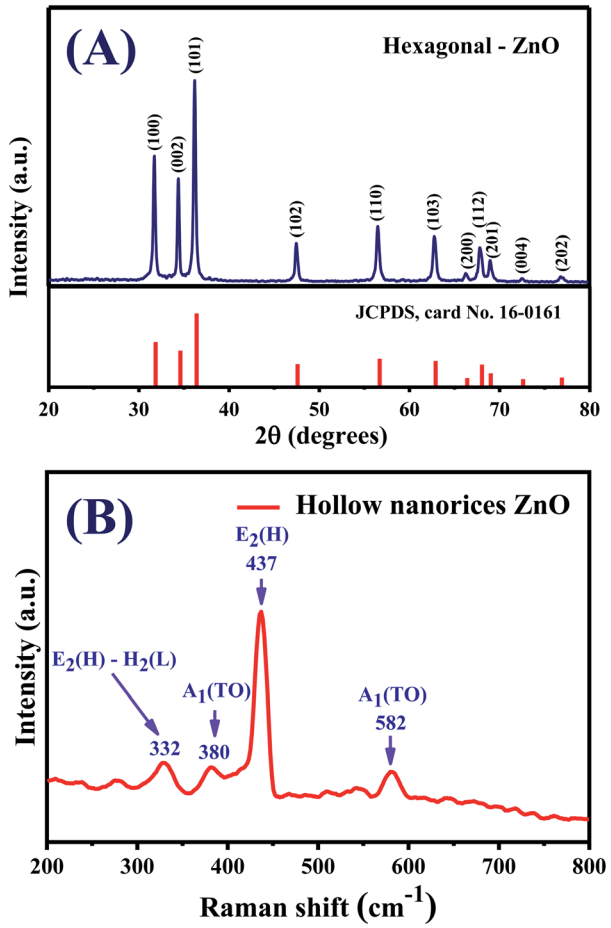

Fig. 3 (A) XRD pattern, (B) Raman spectrum of hollow ZnO nanorices.

the approximate current is linearly proportional to the magnitude of the applied bias voltage (from −7 V to 7 V) over a temperature range of 100–400 °C. This result reveals that the contact between the hollow ZnO nanorices and the Pt electrode is ohmic. Ohmic contact is crucial to the electrical properties of hollow ZnO nanorices with the electrode because the electrical properties of the sensor when exposed to the test gas are properties of the material, not an effect of contact between the hollow ZnO nanorices and the Pt electrode. In the study of Wang *et al.*,[47] the *I–V* characterization of the sensor based on ZnO nanorod arrays with Ag electrode also showed linear results in the applied voltage range from −10 V to 10 V.

Fig. 5B plots the sensor resistance *versus* temperatures measured in dry air, calculated from the *I–V* curves in Fig. 5A. The decrease in resistance of the sensor with increasing temperature occurs because some electrons receive a thermal excitation energy greater than the band gap energy and it jumps from the valence band to the conduction band, the conductivity increases. As the temperature increases, the electron density on the conduction band increases: thus, the conductivity of the semiconductor increases with temperature, and the resistance of the sensor decreases. This result is consistent with the study of Srivastava *et al.*[48] on ZnO nanorods.

The NO_2 sensing properties of the hollow ZnO nanorices were measured at different working temperatures, ranging from 150 °C to 350 °C (Fig. 6). The transient resistance *versus* time of the sensor with exposure to different NO_2 concentrations are shown in Fig. 6A. The sensor's resistance increases upon exposure to NO_2 gas (100 ppb ÷ 2 ppm) and recovers to the based value when the sensor is refreshed with dry air. These results indicate that the adsorption of NO_2 molecules on the surface of the hollow ZnO nanorices is a reversible process. The result is consistent with the study of Mingzhi *et al.*[49] on ZnO nanorods based NO_2 gas sensor, confirming the n-type semiconducting properties of ZnO.

The response time ($\tau_{90\%}$) and recovery ($\tau_{10\%}$) of the sensor were calculated from the resistance–time curves at 1 ppm NO_2 concentration. The response and recovery time of the sensor at different operating temperatures shown in Fig. 6B document that the response and recovery time decrease as the working temperature increases. The response/recovery time for 1 ppm NO_2 at working temperatures of 150 °C, 200 °C, 250 °C, and 300 °C are 214 s/225 s, 194 s/173 s, 175 s/140 s, and 115 s/60 s, respectively. The results are consistent with the finding by Hamaguchi *et al.*,[49] where they reported that as the working temperature of the sensor increases, the recovery and response time decrease. The response and recovery time of few minutes at all operating temperatures; thus, the sensor can be applied for the real-time monitoring of NO_2 gas in ambient air. Here, the NO_2 sensor based on ZnO nanostructures requires a response and recovery time of a few minutes, but using light irradiation could improve the response and recovery characteristics.[50]

Fig. 6C shows the temperature dependence of sensor response for the detection of 100 ppb, 250 ppb, 500 ppb, 1 ppm, and 2 ppm of NO_2 gas. The sensor exhibited the maximum response value at 200 °C for a given concentration, indicating the optimal working temperature. The bell-shape of sensor response depending on working temperature is consistent with other reports.[51] The optimal working temperature value of the

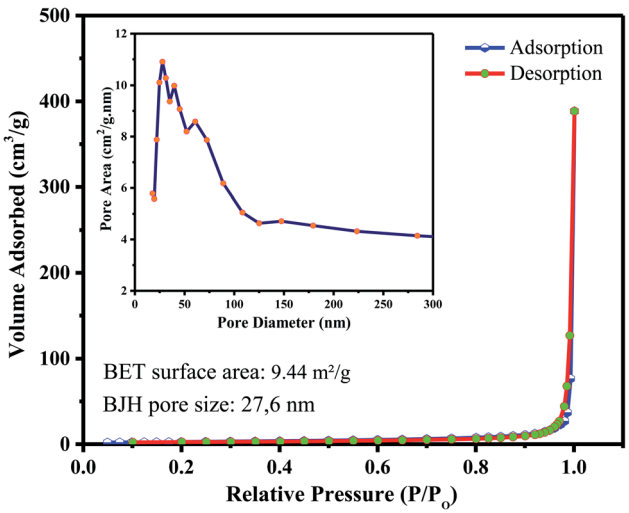

Fig. 4 Typical N_2 adsorption–desorption isotherm of the hollow ZnO nanorices. Inset is the BJH pore size distribution.

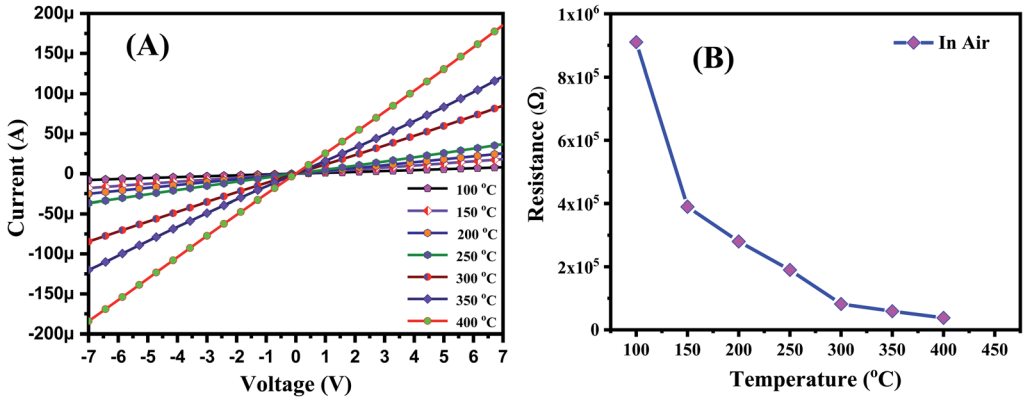

Fig. 5 (A) *I–V* curves of the sensor measured in air at different temperatures and (B) the temperature dependence of the sensor resistance.

hollow nanorice sensor in this study is approximately 100 °C lower than that of the sensor using ZnO nanorods synthesized by the hydrothermal method.[52] The plots of sensor response *versus* NO_2 concentrations at different operating temperatures are shown in Fig. 6D. The survey results show that the sensor response is linearly dependent to NO_2 concentration in the range of 100 ppb ÷ 2 ppm. Therefore, linear electronic circuits can be used for the sensor to measure and control NO_2 toxic gas.

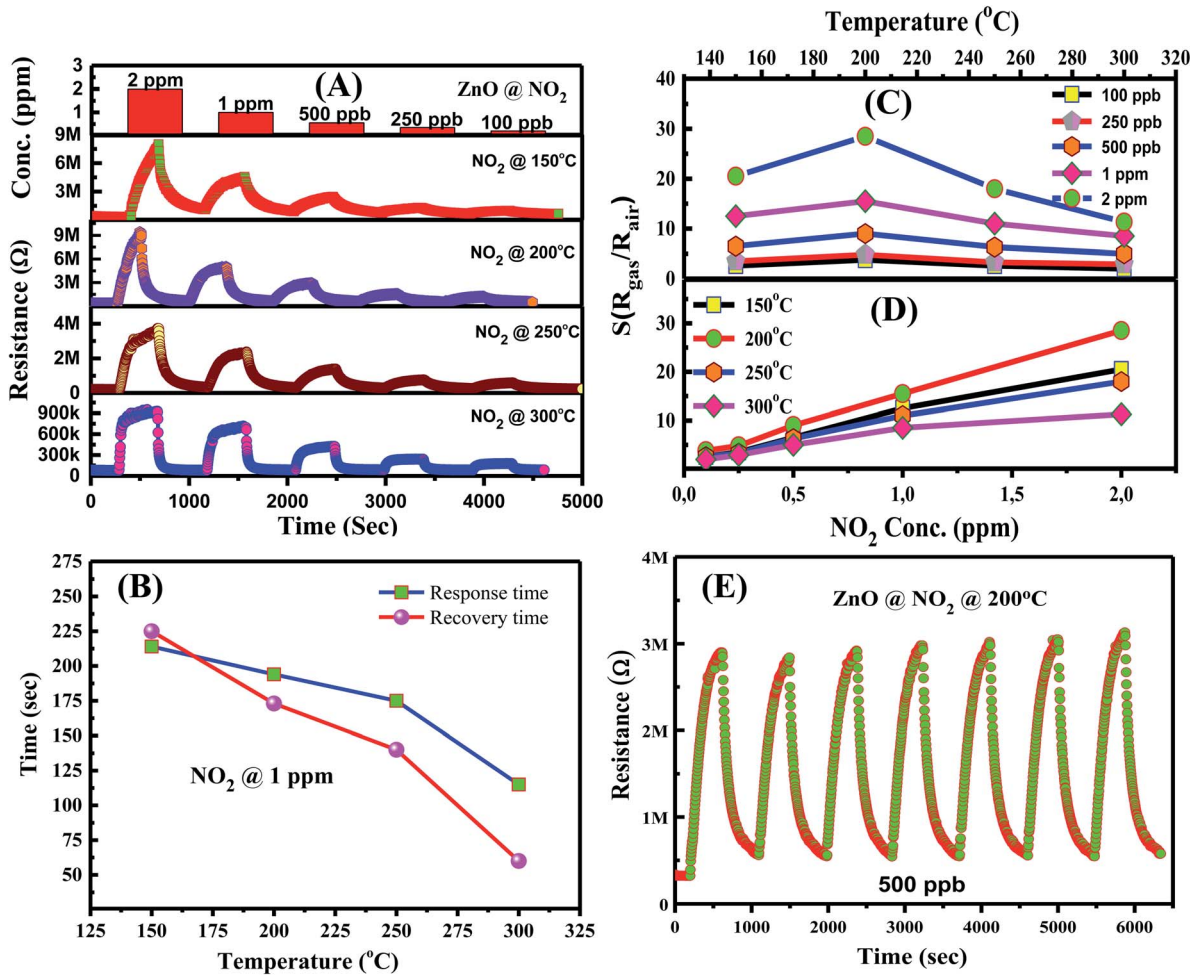

Fig. 6 NO_2-sensing characteristics of hollow ZnO nanorices measured at different temperatures: (A) transient resistance *versus* time upon exposure to different NO_2 concentrations; (B) response and recovery time as functions of the working temperatures measured at 1 ppm concentration NO_2; sensor response, (C) temperature dependence, and (D) concentration dependence of the sensor; (E) repeatability of the sensor.

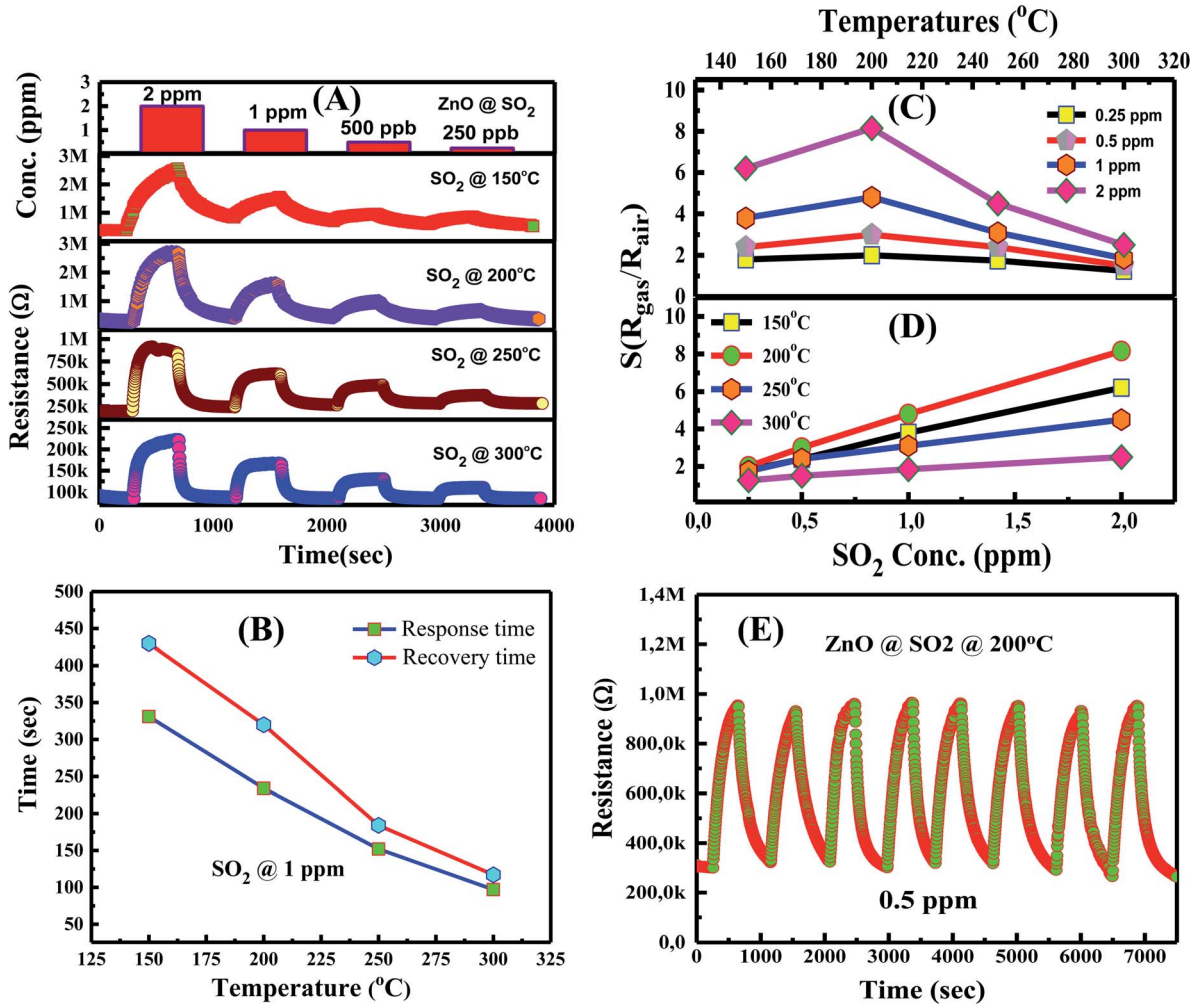

Fig. 7 SO_2-sensing characteristics of hollow ZnO nanorices measured at different temperatures: (A) transient resistance *versus* time upon exposure to different SO_2 concentrations; (B) response and recovery time as functions of the working temperatures measured at 1 ppm concentration SO_2; sensor response, (C) temperature dependence, and (D) concentration dependence of the sensor; (E) repeatability of the sensor.

Repeatability is an important characteristic of gas sensors in practical applications. Fig. 6E shows the transient resistance of the sensor to seven on/off cycle switching from dry air to 1 ppm NO_2 and back to dry air. The sensor exhibits relatively good repeatability after seven on/off cycles, without significant reduction in response value. This result is appointed to the reversible adsorption process of gas molecules on the surface of hollow ZnO nanorices. Anyhow, the long-term stability of the sensor needs to be further investigated so that it can be applied in real measurement systems.

The gas sensing characteristics of the hollow nanorice sensor for the detection of SO_2 gas at different temperatures were also studied. The transient resistance *versus* time as a function of SO_2 concentrations (250 ppb, 500 ppb, 1 ppm, and 2 ppm) measured at 150–300 °C is shown in Fig. 7A. Similar to the response to NO_2 gas, the resistance of the sensor increases when exposed to SO_2 gas and returns to the initial value when exposed to dry air, indicating good response and recovery characteristics. The response and recovery time of the sensor for the detection of 1 ppm SO_2 concentration at different temperatures is shown in Fig. 7B. The response/recovery time of the sensor at working temperatures of 150 °C, 250 °C, 300 °C, and 350 °C are 331 s/430 s, 234 s/320 s, 152 s/184 s, and 97 s/117 s, respectively. The response and recovery time of the sensor decreases with the increase in working temperature, consistent with the previous results for ZnO thin films for NO_2 and H_2S[53] or porous In_2O_3 spheres for H_2.[54] Fig. 7C shows the dependence of sensor response (R_{gas}/R_{air}) on temperature for the detection of 250 ppb, 500 ppb, 1 ppm, and 2 ppm SO_2 concentrations. The sensor also exhibits the optimal working temperature of 200 °C. At an optimum working temperature, the response value is 2.1, 3.1, 4.8, and 8.2 for 250 ppb, 500 ppb, 1 ppm, and 2 ppm SO_2 concentration, respectively. Our results are relatively good compared with other reports. For example, Zhou *et al.*,[35] reported that the sensor based on ZnO nanoflowers has a response value of 6 for 5 ppm SO_2 at 250 °C. Zhou *et al.*[55] reported that the NiO–ZnO nanodisk-based sensor exhibits a response value of 7.5 for 5 ppm SO_2 at 240 °C. Clearly, the

Table 1 Summary of NO_2 and SO_2 sensing performance of ZnO n-type semiconductors

Materials	Methods	Concentration	Gas	Working temp.	Response ($S = R_{air}/R_{gas}$)	Ref.
ZnO nanoparticles	Chemical	500 ppb	NO_2	250 °C	14	56
ZnO nanorods	Ultrasonic spray pyrolysis combined with hydrothermal	5 ppm	NO_2	250 °C	200	24
ZnO nanowire arrays	Hydrothermal	5 ppm	NO_2	250 °C	3.3	57
ZnO nanorod arrays	Chemical	20 ppm	NO_2	175 °C	7.5	33
ZnO nanosheets	Hydrothermal	50 ppm	NO_2	170 °C	10.2	58
ZnO nanoneedles	Chemical	8.5 ppm	NO_2	200 °C	0.81	59
ZnO nanorods	Thermal evaporation	100 ppm	NO_2	200 °C	7.22	60
ZnO thin film	Sol–gel	100 ppm	NO_2	200 °C	1.372	61
ZnO nanoflowers	Hydrothermal	5 ppm	SO_2	250 °C	6	35
ZnO thin film	Sol–gel	5 ppm	NO_2	Room temperature	1.1	62
		10 ppm	SO_2		1.35	
NiO–ZnO nanodisks	Hydrothermal	5 ppm	SO_2	240 °C	7.5	55
GO–ZnO nanorods	Hydrothermal	5 ppm	SO_2	25 °C	2.97	63
Hollow ZnO nanorices	Hydrothermal/calcination	250 ppb	NO_2	200 °C	3.5	This work
		500 ppb			6.5	
		1 ppm			15.3	
Hollow ZnO nanorices	Hydrothermal/calcination	250 ppb	SO_2	200 °C	2.1	This work
		500 ppb			3.1	
		1 ppm			4.8	

hollow ZnO nanorice-based sensor has lower optimal working temperature and higher response values. The hollow structure of the ZnO nanorices may have increased the gas adsorption capacity, which causes the higher response of our sensor.

The plots of sensor response *versus* SO_2 concentrations at working temperatures of 150 °C, 200 °C, 250 °C, and 300 °C is shown in Fig. 7D. The sensor response increases linearly with SO_2 concentration (250 ppb to 2 ppm) in the measured range at all working temperatures. This trend is advantageous in practical applications in preparing the sensor instrument because linear electronic circuits can be used to measure SO_2 in the above concentration range. Fig. 7E is the repeatability of the sensor after eight on/off cycles from dry air to SO_2 and back to dry air. The sensor also exhibits relatively good stability after eight measurement cycles, indicating that the SO_2 adsorption on the surface of hollow ZnO nanorices is a reversible process.

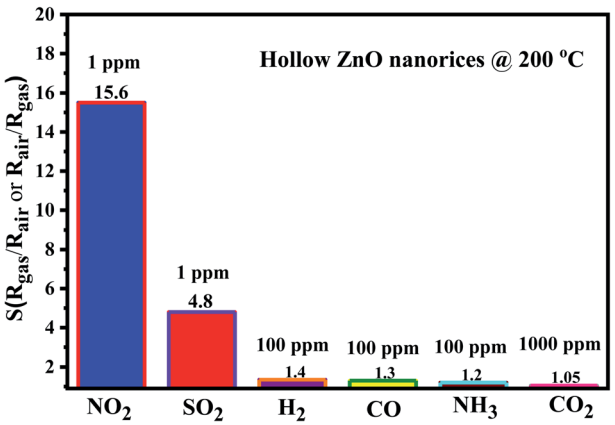

Fig. 8 Selectivity of the sensor to different gases measured at 200 °C.

To understand further the influence of the morphology and characteristics of ZnO hollow nanorices on the NO_2 and SO_2 responses, our results were compared with other reports using different nanostructures, as summarized in Table 1. ZnO nanoparticles demonstrate the highest response, followed by hollow ZnO nanorices, nanorods, nanowire arrays, and thin films.

The selectivity of the sensor over the detection of different gases (NO_2, SO_2, H_2, CO, NH_3, and CO_2) measured at an optimum working temperature of 200 °C is shown in Fig. 8. The results show that the sensor exhibits the highest response to NO_2 among the tested gases. At a concentration of 1 ppm and at a working temperature of 200 °C, the response value for NO_2 is 15.3, whereas that for SO_2 is 4.8. However, the response values for 100 ppm reducing gases, including that for H_2, CO, NH_3, and CO_2, are 1.4, 1.3, 1.2, and 1.05, respectively. Our research results confirm that the sensor based on hollow ZnO nanorices can be applied for NO_2 and SO_2 gas detection and measurement in air pollution.

3.3. Gas sensing mechanism

To explain the increase in sensor resistance upon exposure to NO_2 and SO_2 in comparison with that in dry air, we considered the adsorption of tested gases and oxygen molecules on the surface of hollow ZnO nanorices. During measurement in air as reference, oxygen species adsorb on the surface of the sensing material to form preabsorbed oxygen ions, such as (O_2^-, O^-, O^{2-}) depending on the working temperature of the sensor. The types of oxygen ions adsorbed on the surface of the sensing material can be described by the following reaction equations:[64]

$$O_2(gas) \rightarrow O_2(ads) \quad (5)$$

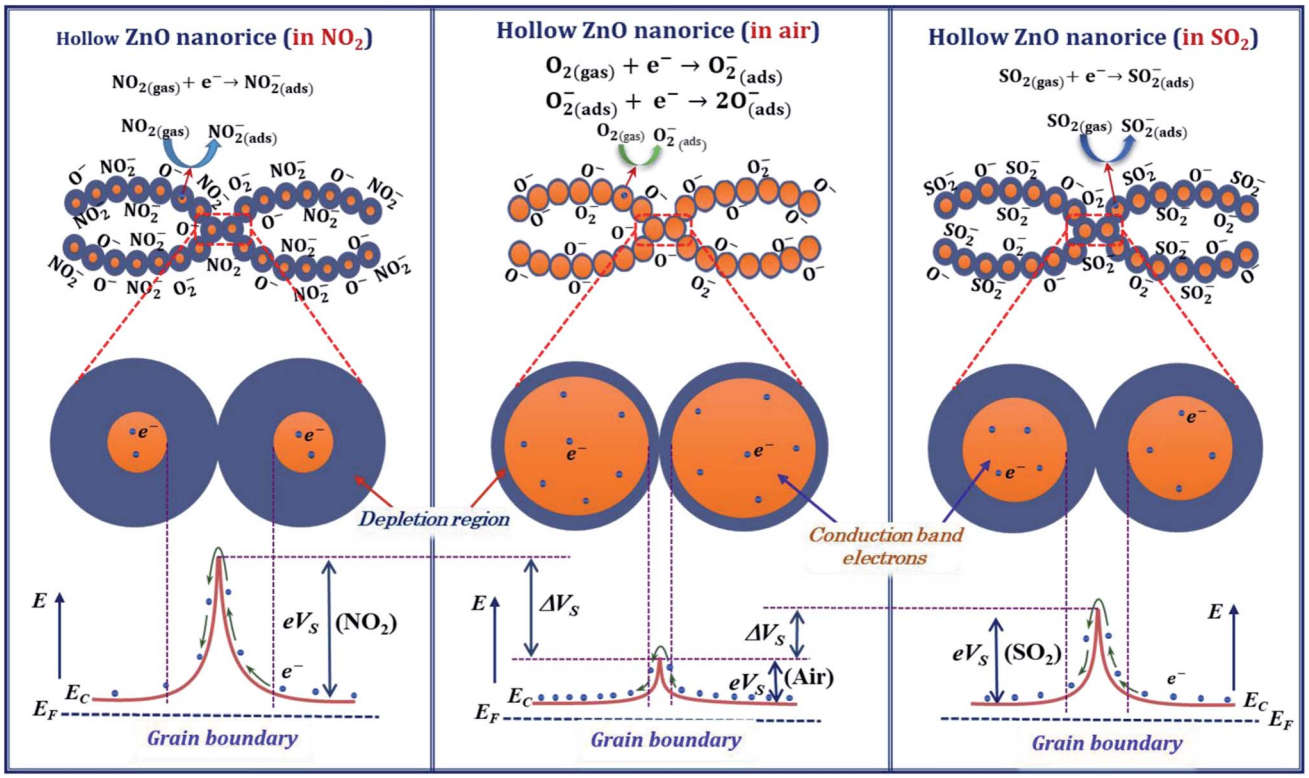

Fig. 9 Illustration the NO_2 and SO_2 gas sensing mechanism of the hollow ZnO nanorices based sensor.

$$O_2(ads) + e^- \rightarrow O_2^-(ads) \quad (6)$$

$$O_2^-(ads) + e^- \rightarrow 2O^-(ads) \quad (7)$$

$$O^-(ads) + e^- \rightarrow O^{2-}(ads) \quad (8)$$

The preabsorbed oxygen species captures electrons and forms a depletion region on the surface of the hollow ZnO nanorices. Given that NO_2 molecule has a higher electron affinity (2.28 eV) than oxygen (0.43 eV),[65] thus, upon exposure to test gas, the NO_2 molecules can adsorb directly on the surface of ZnO, or through the preabsorbed oxygen species. The adsorption of NO_2 gas on the surface of the ZnO material is complex and can be expressed by the following equations:[50]

$$NO_2(gas) + e^- \rightarrow NO_2^-(ads) \quad (9)$$

$$NO_2^-(ads) + O_2^-(ads) + e^- \rightarrow 2O^-(ads) + NO_2^-(ads) \quad (10)$$

$$NO_2^-(ads) + O^-(ads) + 2e^- \rightarrow 2O^{2-}(ads) + NO(gas) \quad (11)$$

$$NO_2^-(ads) + h^+ \rightarrow NO_2(gas) \quad (12)$$

The NO_2 molecules capture more electrons and thus expand the depletion region, as shown in Fig. 9, and result in the increase in sensor resistance.

However, the adsorption of NO_2 molecule on the surface of ZnO is more complex because it depends on the intrinsic defects such as zinc interstitial (Zn_i), zinc vacancy (V_{Zn}), oxygen interstitial (O_i), oxygen vacancy (V_O), oxygen antisite (O_{Zn}) and Zn antisite (Zn_O).[66] Mei Chen *et al.* studied the adsorption of NO_2 molecule on the surface of ZnO material by diffuse reflectance infrared Fourier transform spectroscopy, and X-ray photoelectron spectroscopy,[67] and they pointed out that the intensity of the donors (V_O and Zn_i) and the surface oxygen species (O_2^- and O^{2-}) determine the sensing performance of ZnO. In such report, the oxygen molecule can adsorb on the oxygen vacancy, whereas the NO_2 adsorbs on the zinc interstitial causing the electron transfer. As a result, the sensor resistance increases with exposure to NO_2 gas.

Here, the ZnO nanorices with thin shell and hollow structure can provide large adsorption sites for gas adsorption and thus can increase the sensor response. At an optimum working temperature (200 °C), the response of the ZnO nanorice sensor is 15.3 for 1 ppm NO_2 concentration. This value is approximately seven folds higher than that of the sensor based on ZnO nanowire arrays at an optimum working temperature of 250 °C. This result shows that the sensor using hollow ZnO nanorice materials can improve the response and reduce the optimal working temperature simultaneously. Therefore, the hollow or porous nanostructures can improve sensor response and detect gases at lower concentrations simultaneously.

The SO_2 sensing mechanism of metal oxide-based gas sensors is relatively complex because SO_2 simultaneously oxidizes and reduces gas, depending on the tested conditions. In a study reported by Tyagi *et al.*,[68] the resistance of the SnO_2 thin film (n-type) decreases when exposed to SO_2 gas. The SO_2 gas molecules interact with the preabsorbed oxygen ion (O^{2-})

on the surface of the SnO_2 film and return electrons to the conduction band, resulting in the decrease in sensor resistance, according to the following equation:

$$SO_2(gas) + O^- \rightarrow SO_3(ads) + e^- \quad (13)$$

However, in the report of Boudiba *et al.*,[11] the n-type WO_3 produces the opposite result, where the resistance of the sensor increases when exposed to 5 ppm SO_2 at a working temperature of 260 °C. In addition, according to a report[69] on a pure WO_3-based sensor, upon exposure to 800 ppm SO_2, the sensor resistance increases in the temperature range of 350–500 °C, but it decreases when the temperature is higher than 500 °C. Such results show that SO_2 gas acts as an electron acceptor (oxidizing gas) or electron donor (reducing gas) depending on the working temperature of the sensor. This result is similar to that of the pure SnO_2, and the 1% Cu–SnO_2 sensors,[70] which when exposed to 6 ppm SO_2, the resistance of the sensor increases in the temperature range of 225–275 °C and decreases in the temperature range of 300–350 °C.

In our study, we believe that SO_2 exhibits oxidizing properties by directly adsorbing on the surface of the hollow ZnO nanorices, which may be the main cause of the increase in the resistance of the sensor when exposed to SO_2. The process of SO_2 adsorption and electron capture is described by the following equation:[2]

$$SO_2(gas) + e^- \rightarrow SO_2^-(ads) \quad (14)$$

After being refreshed with dry air, the adsorbed SO_2 gas molecules desorb from the surface of the hollow ZnO nanorices and return electrons to the conduction band of ZnO, thus allow the resistance of the sensor to recover to the initial value. The desorption speed is faster at a higher working temperature. This result is similar to our previous report[71] on a sensor using CuO (p-type) nanoplates. The resistance of the sensor increases when exposed to SO_2 and returns to the based value when the sensor is refreshed with dry air. To conclusion, in our study, the hollow structure and thin shell thickness of the nanorice responses for the high sensitivity of the sensor. As shown in Fig. 9, the adsorption of NO_2, and SO_2 molecules on the surface of ZnO nanorices captures electrons from the conduction band and thus change the depletion region compared with that in air. Therefore, the resistance of the sensor increases significantly with introduction of NO_2 and SO_2 gases.

4. Conclusion

For the first time, we have successfully fabricated hollow ZnO nanorices by a simple hydrothermal method without using surfactants for NO_2 and SO_2 gas sensor application. The hollow ZnO nanorices have an average length and diameter of approximately 500 and 160 nm, respectively. The nanorices have a thin shell with a thickness of approximately 20 nm. The surface of the hollow ZnO nanorices is not smooth due to the accumulation of crystalline nanoparticles. The specific surface area of the hollow ZnO nanorices is relatively large (approximately 9.44 $m^2 g^{-1}$), whereas the average pore diameter is approximately 30 nm. The formation of hollow ZnO nanorices can be attributed to the agglomeration of glucose molecules into the soft-template with a rice-like morphology. During the hydrothermal process, the precursors decomposed to form ZnO crystals and assembled on the surface of the glucose template in the shape of nanorices. After the removal of the glucose soft template, hollow nanorices are obtained. Hollow ZnO nanorices are suitable for fabrication of sensors to detect NO_2 and SO_2 gases at the ppb level. Our results show that the fabricated sensor based on hollow ZnO nanorices can be applied to the monitoring, detection, and measurement of toxic NO_2 and SO_2 gases in air pollution.

Conflicts of interest

There are no conflicts to declare.

Acknowledgements

This research is funded by the Vietnam National Foundation for Science and Technology Development (Nafosted, code: 103.02-2018.07).

References

1 S. Das, S. Chakraborty, O. Parkash, D. Kumar, S. Bandyopadhyay, S. K. Samudrala, *et al.*, Vanadium doped tin dioxide as a novel sulfur dioxide sensor, *Talanta*, 2008, **75**, 385–389, DOI: 10.1016/j.talanta.2007.11.010.

2 R. Kumar, D. K. Avasthi and A. Kaur, Fabrication of chemiresistive gas sensors based on multistep reduced graphene oxide for low parts per million monitoring of sulfur dioxide at room temperature, *Sens. Actuators, B*, 2017, **242**, 461–468, DOI: 10.1016/j.snb.2016.11.018.

3 P. Van Tong, N. D. Hoa, V. Van Quang, N. Van Duy and N. Van Hieu, Diameter controlled synthesis of tungsten oxide nanorod bundles for highly sensitive NO2 gas sensors, *Sens. Actuators, B*, 2013, **183**, 372–380, DOI: 10.1016/j.snb.2013.03.086.

4 C. Li, L. Yu, X. Fan, M. Yin, N. Nan, L. Cui, *et al.*, Nucleation density and pore size tunable growth of ZnO nanowalls by a facile solution approach: growth mechanism and NO2 gas sensing properties, *RSC Adv.*, 2020, **10**, 3319–3328, DOI: 10.1039/C9RA07933E.

5 M. Zhao, F. Dong, L. Yan, L. Xu, X. Zhang, P. Chen, *et al.*, High efficiency room temperature detection of NO2 gas based on ultrathin metal/graphene devices, *RSC Adv.*, 2016, **6**, 84082–84089, DOI: 10.1039/C6RA16863A.

6 P. Zhou, Y. Shen, W. Lu, S. Zhao, T. Li, X. Zhong, *et al.*, Highly selective NO2 chemiresistive gas sensor based on hierarchical In2O3 microflowers grown on clinoptilolite substrates, *J. Alloys Compd.*, 2020, **828**, 154395, DOI: 10.1016/j.jallcom.2020.154395.

7 S. C. Lee, B. W. Hwang, S. J. Lee, H. Y. Choi, S. Y. Kim, S. Y. Jung, *et al.*, A novel tin oxide-based recoverable thick film SO2 gas sensor promoted with magnesium and

vanadium oxides, *Sens. Actuators, B*, 2011, **160**, 1328–1334, DOI: 10.1016/j.snb.2011.09.070.

8 J. W. Fergus, A review of electrolyte and electrode materials for high temperature electrochemical CO2 and SO2 gas sensors, *Sens. Actuators, B*, 2008, **134**, 1034–1041, DOI: 10.1016/j.snb.2008.07.005.

9 Y. J. Lee, H. B. Kim, Y. R. Roh, H. M. Cho and S. Baik, Development of a saw gas sensor for monitoring so2 gas, *Sens. Actuators, A*, 1998, **64**, 173–178, DOI: 10.1016/S0924-4247(98)80011-3.

10 T. M. Razek, M. J. Miller, S. S. Hassan and M. A. Arnold, Optical sensor for sulfur dioxide based on fluorescence quenching, *Talanta*, 1999, **50**, 491–498, DOI: 10.1016/S0039-9140(99)00151-4.

11 A. Boudiba, C. Zhang, C. Bittencourt, P. Umek, M.-G. Olivier, R. Snyders, *et al.*, SO2 Gas Sensors based on WO3 Nanostructures with Different Morphologies, *Procedia Eng.*, 2012, **47**, 1033–1036, DOI: 10.1016/j.proeng.2012.09.326.

12 B. Zhang, N. Bao, T. Wang, Y. Xu, Y. Dong, Y. Ni, *et al.*, High-performance room temperature NO2 gas sensor based on visible light irradiated In2O3 nanowires, *J. Alloys Compd.*, 2021, **867**, 159076, DOI: 10.1016/j.jallcom.2021.159076.

13 J. Hu, Y. Liang, Y. Sun, Z. Zhao, M. Zhang, P. Li, *et al.*, Highly sensitive NO2 detection on ppb level by devices based on Pd-loaded In2O3 hierarchical microstructures, *Sens. Actuators, B*, 2017, **252**, 116–126, DOI: 10.1016/j.snb.2017.05.113.

14 N. Van Toan, N. Viet Chien, N. Van Duy, H. Si Hong, H. Nguyen, N. Duc Hoa, *et al.*, Fabrication of highly sensitive and selective H2 gas sensor based on SnO2 thin film sensitized with microsized Pd islands, *J. Hazard. Mater.*, 2016, **301**, 433–442, DOI: 10.1016/j.jhazmat.2015.09.013.

15 A. Vomiero, S. Bianchi, E. Comini, G. Faglia, M. Ferroni, N. Poli, *et al.*, In2O3 nanowires for gas sensors: morphology and sensing characterisation, *Thin Solid Films*, 2007, **515**, 8356–8359, DOI: 10.1016/j.tsf.2007.03.034.

16 Y. S. Haiduk, A. A. Khort, N. M. Lapchuk and A. A. Savitsky, Study of WO3 –In2O3 nanocomposites for highly sensitive CO and NO2 gas sensors, *J. Solid State Chem.*, 2019, **273**, 25–31, DOI: 10.1016/j.jssc.2019.02.023.

17 S. Zhao, Y. Shen, P. Zhou, X. Zhong, C. Han, Q. Zhao, *et al.*, Design of Au@WO3 core−shell structured nanospheres for ppb-level NO2 sensing, *Sens. Actuators, B*, 2019, **282**, 917–926, DOI: 10.1016/j.snb.2018.11.142.

18 D. D. Trung, N. D. Hoa, P. V. Tong, N. V. Duy, T. D. Dao, H. V. Chung, *et al.*, Effective decoration of Pd nanoparticles on the surface of SnO2 nanowires for enhancement of CO gas-sensing performance, *J. Hazard. Mater.*, 2014, **265**, 124–132, DOI: 10.1016/j.jhazmat.2013.11.054.

19 S. Das, K. G. Girija, A. K. Debnath and R. K. Vatsa, Enhanced NO2 and SO2 sensor response under ambient conditions by polyol synthesized Ni doped SnO2 nanoparticles, *J. Alloys Compd.*, 2021, **854**, 157276, DOI: 10.1016/j.jallcom.2020.157276.

20 A. Mirzaei, S. S. Kim and H. W. Kim, Resistance-based H2S gas sensors using metal oxide nanostructures: A review of recent advances, *J. Hazard. Mater.*, 2018, **357**, 314–331, DOI: 10.1016/j.jhazmat.2018.06.015.

21 F. Lu, W. Cai and Y. Zhang, ZnO Hierarchical Micro/Nanoarchitectures: Solvothermal Synthesis and Structurally Enhanced Photocatalytic Performance, *Adv. Funct. Mater.*, 2008, **18**, 1047–1056, DOI: 10.1002/adfm.200700973.

22 Y. Kang, F. Yu, L. Zhang, W. Wang, L. Chen and Y. Li, Review of ZnO-based nanomaterials in gas sensors, *Solid State Ionics*, 2021, **360**, 115544, DOI: 10.1016/j.ssi.2020.115544.

23 Z. Liu, L. Yu, F. Guo, S. Liu, L. Qi, M. Shan, *et al.*, Facial development of high performance room temperature NO2 gas sensors based on ZnO nanowalls decorated rGO nanosheets, *Appl. Surf. Sci.*, 2017, **423**, 721–727, DOI: 10.1016/j.apsusc.2017.06.160.

24 F.-T. Liu, S.-F. Gao, S.-K. Pei, S.-C. Tseng and C.-H. J. Liu, ZnO nanorod gas sensor for NO2 detection, *J. Taiwan Inst. Chem. Eng.*, 2009, **40**, 528–532, DOI: 10.1016/j.jtice.2009.03.008.

25 B. Yuliarto, M. F. Ramadhani, Nugraha, N. L. W. Septiani and K. A. Hamam, Enhancement of SO2 gas sensing performance using ZnO nanorod thin films: the role of deposition time, *J. Mater. Sci.*, 2017, **52**, 4543–4554, DOI: 10.1007/s10853-016-0699-5.

26 N. D. Khoang, H. S. Hong, D. D. Trung, N. V. Duy, N. D. Hoa, D. D. Thinh, *et al.*, On-chip growth of wafer-scale planar-type ZnO nanorod sensors for effective detection of CO gas, *Sens. Actuators, B*, 2013, **181**, 529–536, DOI: 10.1016/j.snb.2013.02.047.

27 P. Sundara Venkatesh, P. Dharmaraj, V. Purushothaman, V. Ramakrishnan and K. Jeganathan, Point defects assisted NH3 gas sensing properties in ZnO nanostructures, *Sens. Actuators, B*, 2015, **212**, 10–17, DOI: 10.1016/j.snb.2015.01.070.

28 R. Javed, M. Usman, S. Tabassum and M. Zia, Effect of capping agents: Structural, optical and biological properties of ZnO nanoparticles, *Appl. Surf. Sci.*, 2016, **386**, 319–326, DOI: 10.1016/j.apsusc.2016.06.042.

29 S. Tuscharoen, N. Kulakeatmongkol, M. Horprathum, K. Aiampanakit, P. Eiamchai, V. Pattantsetakul, *et al.*, Low-temperature hydrothermal synthesis single-crystal ZnO nanowire for gas sensor application, *Mater. Today: Proc.*, 2018, **5**, 15213–15217, DOI: 10.1016/j.matpr.2018.04.085.

30 L. Van Duy, N. Van Duy, C. M. Hung, N. D. Hoa and N. Q. Dich, Urea mediated synthesis and acetone-sensing properties of ultrathin porous ZnO nanoplates, *Mater. Today Commun.*, 2020, **25**, 101445, DOI: 10.1016/j.mtcomm.2020.101445.

31 Y. Xi, C. G. Hu, X. Y. Han, Y. F. Xiong, P. X. Gao and G. B. Liu, Hydrothermal synthesis of ZnO nanobelts and gas sensitivity property, *Solid State Commun.*, 2007, **141**, 506–509, DOI: 10.1016/j.ssc.2006.12.016.

32 M. Jiao, N. V. Chien, N. V. Duy, N. D. Hoa, N. V. Hieu, K. Hjort, *et al.*, On-chip hydrothermal growth of ZnO nanorods at low temperature for highly selective NO2 gas sensor, *Mater. Lett.*, 2016, **169**, 231–235, DOI: 10.1016/j.matlet.2016.01.123.

33 S. A. Vanalakar, V. L. Patil, N. S. Harale, S. A. Vhanalakar, M. G. Gang, J. Y. Kim, *et al.*, Controlled growth of ZnO nanorod arrays *via* wet chemical route for NO2 gas sensor applications, *Sens. Actuators, B*, 2015, **221**, 1195–1201, DOI: 10.1016/j.snb.2015.07.084.

34 M. Jiao, N. Van Duy, D. D. Trung, N. D. Hoa, N. Van Hieu, K. Hjort, *et al.*, Comparison of NO2 Gas-Sensing Properties of Three Different ZnO Nanostructures Synthesized by On-Chip Low-Temperature Hydrothermal Growth, *J. Electron. Mater.*, 2018, **47**, 785–793, DOI: 10.1007/s11664-017-5829-6.

35 Q. Zhou, B. Xie, L. Jin, W. Chen and J. Li, *Hydrothermal Synthesis and Responsive Characteristics of Hierarchical Zinc Oxide Nanoflowers to Sulfur Dioxide 2016*, 2016.

36 A. Umar, A. A. Ibrahim, R. Kumar, H. Algadi, H. Albargi, M. A. Alsairi, *et al.*, CdO–ZnO nanorices for enhanced and selective formaldehyde gas sensing applications, *Environ. Res.*, 2021, **200**, 111377, DOI: 10.1016/j.envres.2021.111377.

37 P. Van Tong, L. Hoang Minh, N. Van Duy and C. Manh Hung, Porous In2O3 nanorods fabricated by hydrothermal method for an effective CO gas sensor, *Mater. Res. Bull.*, 2021, **137**, 111179, DOI: 10.1016/j.materresbull.2020.111179.

38 P. Van Tong, N. D. Hoa, N. Van Duy, D. T. T. Le and N. Van Hieu, Enhancement of gas-sensing characteristics of hydrothermally synthesized WO3 nanorods by surface decoration with Pd nanoparticles, *Sens. Actuators, B*, 2016, **223**, 453–460, DOI: 10.1016/j.snb.2015.09.108.

39 Y. Liang, N. Guo, L. Li, R. Li, G. Ji and S. Gan, Preparation of porous 3D Ce-doped ZnO microflowers with enhanced photocatalytic performance, *RSC Adv.*, 2015, **5**, 59887–59894, DOI: 10.1039/C5RA08519E.

40 E. A. Araújo, F. X. Nobre, G. D. S. Sousa, L. S. Cavalcante, M. Rita De Morais Chaves Santos, F. L. Souza, *et al.*, Synthesis, growth mechanism, optical properties and catalytic activity of ZnO microcrystals obtained *via* hydrothermal processing, *RSC Adv.*, 2017, **7**, 24263–24281, DOI: 10.1039/c7ra03277c.

41 X. Chen, X. Jing, J. Wang, J. Liu, D. Song and L. Liu, Self-assembly of ZnO nanoparticles into hollow microspheres *via* a facile solvothermal route and their application as gas sensor, *CrystEngComm*, 2013, **15**, 7243–7249, DOI: 10.1039/c3ce40654g.

42 R. Bomila, S. Srinivasan, A. Venkatesan, B. Bharath and K. Perinbam, Structural, optical and antibacterial activity studies of Ce-doped ZnO nanoparticles prepared by wet-chemical method, *Mater. Res. Innovations*, 2018, **22**, 379–386, DOI: 10.1080/14328917.2017.1324379.

43 T. Bora, D. Zoepfl and J. Dutta, Importance of Plasmonic Heating on Visible Light Driven Photocatalysis of Gold Nanoparticle Decorated Zinc Oxide Nanorods, *Sci. Rep.*, 2016, **6**, 26913, DOI: 10.1038/srep26913.

44 A. Moulahi, F. Sediri and N. Gharbi, Hydrothermal synthesis of nanostructured zinc oxide and study of their optical properties, *Mater. Res. Bull.*, 2012, **47**, 667–671, DOI: 10.1016/j.materresbull.2011.12.027.

45 K. A. Cychosz and M. Thommes, Progress in the Physisorption Characterization of Nanoporous Gas Storage Materials, *Engineering*, 2018, **4**, 559–566, DOI: 10.1016/j.eng.2018.06.001.

46 R. K. Saha, M. K. Debanath, B. Paul, S. Medhi and E. Saikia, Antibacterial and nonlinear dynamical analysis of flower and hexagon-shaped ZnO microstructures, *Sci. Rep.*, 2020, **10**, 2598, DOI: 10.1038/s41598-020-59534-x.

47 X. Wang, F. Sun, Y. Duan, Z. Yin, W. Luo, Y. Huang, *et al.*, Highly sensitive, temperature-dependent gas sensor based on hierarchical ZnO nanorod arrays, *J. Mater. Chem. C*, 2015, **3**, 11397–11405, DOI: 10.1039/C5TC02187A.

48 R. Srivastava, Investigation on Temperature Sensing of Nanostructured Zinc Oxide Synthesized *via* Oxalate Route, *J. Sens. Technol.*, 2012, **02**, 8–12, DOI: 10.4236/jst.2012.21002.

49 T. Hamaguchi, N. Yabuki, M. Uno, S. Yamanaka, M. Egashira, Y. Shimizu, *et al.*, Synthesis and H2 gas sensing properties of tin oxide nanohole arrays with various electrodes, *Sens. Actuators, B*, 2006, **113**, 852–856, DOI: 10.1016/j.snb.2005.03.062.

50 J. Xuan, G. Zhao, M. Sun, F. Jia, X. Wang, T. Zhou, *et al.*, Low-temperature operating ZnO-based NO 2 sensors: a review, *RSC Adv.*, 2020, **10**, 39786–39807, DOI: 10.1039/D0RA07328H.

51 A. Mirzaei, J.-H. Lee, S. M. Majhi, M. Weber, M. Bechelany, H. W. Kim, *et al.*, Resistive gas sensors based on metal-oxide nanowires, *J. Appl. Phys.*, 2019, **126**, 241102, DOI: 10.1063/1.5118805.

52 L. Shi, A. J. T. Naik, J. B. M. Goodall, C. Tighe, R. Gruar, R. Binions, *et al.*, Highly Sensitive ZnO Nanorod- and Nanoprism-Based NO2 Gas Sensors: Size and Shape Control Using a Continuous Hydrothermal Pilot Plant, *Langmuir*, 2013, **29**, 10603–10609, DOI: 10.1021/la402339m.

53 R. Nisha, K. N. Madhusoodanan, T. V. Vimalkumar and K. P. Vijayakumar, Gas sensing application of nanocrystalline zinc oxide thin films prepared by spray pyrolysis, *Bull. Mater. Sci.*, 2015, **38**, 583–591, DOI: 10.1007/s12034-015-0911-2.

54 Z. Li, S. Yan, Z. Wu, H. Li, J. Wang, W. Shen, *et al.*, Hydrogen gas sensor based on mesoporous In2O3 with fast response/recovery and ppb level detection limit, *Int. J. Hydrogen Energy*, 2018, **43**, 22746–22755, DOI: 10.1016/j.ijhydene.2018.10.101.

55 Q. Zhou, W. Zeng, W. Chen, L. Xu, R. Kumar and A. Umar, High sensitive and low-concentration sulfur dioxide (SO2) gas sensor application of heterostructure NiO-ZnO nanodisks, *Sens. Actuators, B*, 2019, **298**, 126870, DOI: 10.1016/j.snb.2019.126870.

56 C. T. Quy, N. X. Thai, N. D. Hoa, D. T. Thanh Le, C. M. Hung, N. Van Duy, *et al.*, C2H5OH and NO2 sensing properties of ZnO nanostructures: correlation between crystal size, defect level and sensing performance, *RSC Adv.*, 2018, **8**, 5629–5639, DOI: 10.1039/C7RA13702H.

57 X. Chen, Y. Shen, W. Zhang, J. Zhang, D. Wei, R. Lu, *et al.*, In-situ growth of ZnO nanowire arrays on the sensing electrode *via* a facile hydrothermal route for high-performance NO2 sensor, *Appl. Surf. Sci.*, 2018, **435**, 1096–1104, DOI: 10.1016/j.apsusc.2017.11.222.

58 T. V. A. Kusumam, V. S. Siril, K. N. Madhusoodanan, M. Prashantkumar, Y. T. Ravikiran and N. K. Renuka, NO2 gas sensing performance of zinc oxide nanostructures synthesized by surfactant assisted Low temperature hydrothermal technique, *Sens. Actuators, A*, 2021, **318**, 112389, DOI: 10.1016/j.sna.2020.112389.

59 R. C. Pawar, J.-W. Lee, V. B. Patil and C. S. Lee, Synthesis of multi-dimensional ZnO nanostructures in aqueous medium for the application of gas sensor, *Sens. Actuators, B*, 2013, **187**, 323–330, DOI: 10.1016/j.snb.2012.11.100.

60 Y. H. Navale, S. T. Navale, N. S. Ramgir, F. J. Stadler, S. K. Gupta, D. K. Aswal, *et al.*, Zinc oxide hierarchical nanostructures as potential NO2 sensors, *Sens. Actuators, B*, 2017, **251**, 551–563, DOI: 10.1016/j.snb.2017.05.085.

61 A. Z. Sadek, S. Choopun, W. Wlodarski, S. J. Ippolito and K. Kalantar-zadeh, Characterization of ZnO Nanobelt-Based Gas Sensor for H2, NO2, and Hydrocarbon Sensing, *IEEE Sens. J.*, 2007, **7**, 919–924, DOI: 10.1109/JSEN.2007.895963.

62 A. Gaiardo, B. Fabbri, A. Giberti, V. Guidi, P. Bellutti, C. Malagù, *et al.*, ZnO and Au/ZnO thin films: Room-temperature chemoresistive properties for gas sensing applications, *Sens. Actuators, B*, 2016, **237**, 1085–1094, DOI: 10.1016/j.snb.2016.07.134.

63 V. Dhingra, S. Kumar, R. Kumar, A. Garg and A. Chowdhuri, Room temperature SO2 and H2 gas sensing using hydrothermally grown GO–ZnO nanorod composite films, *Mater. Res. Express*, 2020, **7**, 065012, DOI: 10.1088/2053-1591/ab9ae7.

64 S. Peng, G. Wu, W. Song and Q. Wang, Application of Flower-Like ZnO Nanorods Gas Sensor Detecting Decomposition Products, *J. Nanomater.*, 2013, **2013**, 1–7, DOI: 10.1155/2013/135147.

65 N. D. Hoa, N. Van Quy and D. Kim, Nanowire structured SnOx–SWNT composites: High performance sensor for NOx detection, *Sens. Actuators, B*, 2009, **142**, 253–259, DOI: 10.1016/j.snb.2009.07.053.

66 M. D. McCluskey and S. J. Jokela, Defects in ZnO, *J. Appl. Phys.*, 2009, **106**, 071101, DOI: 10.1063/1.3216464.

67 M. Chen, Z. Wang, D. Han, F. Gu and G. Guo, Porous ZnO Polygonal Nanoflakes: Synthesis, Use in High-Sensitivity NO2 Gas Sensor, and Proposed Mechanism of Gas Sensing, *J. Phys. Chem. C*, 2011, **115**, 12763–12773, DOI: 10.1021/jp201816d.

68 P. Tyagi, A. Sharma, M. Tomar and V. Gupta, Metal oxide catalyst assisted SnO2 thin film based SO2 gas sensor, *Sens. Actuators, B*, 2016, **224**, 282–289, DOI: 10.1016/j.snb.2015.10.050.

69 Y. Shimizu, N. Matsunaga, T. Hyodo and M. Egashira, Improvement of SO2 sensing properties of WO3 by noble metal loading, *Sens. Actuators, B*, 2001, **77**, 35–40, DOI: 10.1016/S0925-4005(01)00669-4.

70 C. Zhao, H. Gong, G. Niu and F. Wang, Ultrasensitive SO2 sensor for sub-ppm detection using Cu-doped SnO2 nanosheet arrays directly grown on chip, *Sens. Actuators, B*, 2020, **324**, 128745, DOI: 10.1016/j.snb.2020.128745.

71 P. Van Tong, N. D. Hoa, H. T. Nha, N. Van Duy, C. M. Hung and N. Van Hieu, SO2 and H2S Sensing Properties of Hydrothermally Synthesized CuO Nanoplates, *J. Electron. Mater.*, 2018, **47**, 7170–7178, DOI: 10.1007/s11664-018-6648-0.